The Variation of Clusters with Increasing Number of Antennas by Virtual Measurement

Chao Wang*, Jianhua Zhang*, Lei Tian*, Mengmeng Liu*, and Ye Wu†
*Key Laboratory of Universal Wireless Communications, Ministry of Education, Wireless Technology Innovation Institute, Beijing University of Posts and Telecommunications, P.O. box # 92, China, 100876
†Huawei Technologies Co., Ltd.
Email: {chaowang, jhzhang}@bupt.edu.cn

***Abstract*—This paper shows the variation of clusters with the increasing number of antennas. The data was collected from the massive MIMO mobile measurement at 3.5 GHz, in line of sight (LoS) and non line of sight (NLoS) conditions, respectively. And the virtual measurement method is used to form the 64-element, 128-element and 256-element virtual antenna array from the 32-element antenna array. After estimating parameters by the space-alternating generalized expectation maximization (SAGE) algorithm and clustering by KPowerMeans algorithm, the parameters of clusters are displayed in angular domain and delay domain. The cluster-level angular power spectrums (APS) are shown, the intra-cluster angular spread (AS) and intra-cluster delay spread (DS) of these 4 groups of data are calculated, to display the clusters' variation when antenna number increases.**

***Index Terms*—massive MIMO, cluster, virtual measurement.**

I. Introduction

Cluster is defined as a group of multipath components (MPCs) with similar parameters, e.g., angle of arrival (AoA), angle of departure (AoD), and delay. For conventional multiple-input multiple-output (MIMO), many measurements have been conducted following by theoretical analysis to study the cluster characteristics, which give a better understanding of the wireless propagation channels [1, 2]. Many wireless channel models are based on the concept of multipath clusters. According to [3], unclustered models tend to overestimate the capacity if the MPCs are indeed clustered. In addition, from an aspect of system level evaluation, it is convenient to model the propagation channel in terms of cluster properties rather than model the behavior of individual MPCs.

Considering this, a lot of studies about cluster-level parameters in different scenarios have been done [4–6]. In 4G era, conventional MIMO technology was used in the channel measurements. Nowadays, more and more work is turning to the massive MIMO technology. Compared to the current state of the art, massive MIMO has a large number of antennas, typically tens or hundreds, which can provide better performance in efficiency, capacity, reliability, etc [7, 8]. A series of massive MIMO measurement campaigns have been performed to evaluate the channel performance. In [9], outdoor channel measurements at 2.6 GHz with a linear virtual array and a cylindrical array of 128-element antenna are reported, which study the sum-rate capacity, spectrum efficiency, precoding schemes and etc. In [10], an outdoor static measurement performed in a stadium with a linear 128-element antenna virtual array at 1.4725 GHz, and the angular power spectrum (APS) in massive MIMO channel is analyzed.

With increasing number of antennas, the characteristics of clusters would probably change in angle domain and delay domain. And these parameters are linked to the channel capacity directly. To the best knowledge of authors, there is still no relevant study on the variation of clusters with different number of antennas.

Considering this, a new massive MIMO mobile measurement campaign in urban macro (UMa) scenario, including line of sight (LoS) and non line of sight (NLoS) propagation conditions, with virtual measurement method at 3.5 GHz and 200 MHz bandwidth are designed and performed. By virtual measurement, the 32-element antenna array can be used to form the 64-element, 128-element and 256-element virtual antenna array. And the corresponding data are analyzed, the propagation condition become better as the antennas become more.

The rest of the paper is organized as follows. In Section II, the channel measurement setup and the method of data processing are described in detail. Section III shows the numerical results and figures in detail. Finally, Section IV concludes the paper.

II. Channel Measurement and Data Processing

To collect massive MIMO mobile channel data, a virtual measurement method is designed to perform this measurement. Then the space-alternating generalized expectation maximization (SAGE) algorithm is used to estimate the channel parameters from the raw data, and the properties of the clusters were extracted by clustering algorithm. More details about the measurement setup and data processing are described in the following.

A. Measurement Description

The mobile measurement was performed in the Hongfu Campus, Beijing University of Posts and Telecommunications (40°06'25" N, 116°22'07" E), a typical UMa scenario (see Fig. 1). Two measurement routes, R1 and R2, corresponding to LoS and NLoS conditions, are designed, respectively. R1 is parallel to the direction of transmitting waves, while R2

Fig. 1. The overview of the measurement area by Baidu Map (The red point is the Tx side, two yellow lines, R1 and R2, represent the measurement route in LoS and NLoS conditions, respectively)

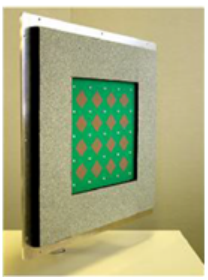

1/5	2/6	3/7	4/8
9/13	10/14	11/15	12/16
17/21	18/22	19/23	20/24
25/29	26/30	27/31	28/32

(a) Tx: 4×4 patches with each patch comprising a pair of cross-polarized antennas.

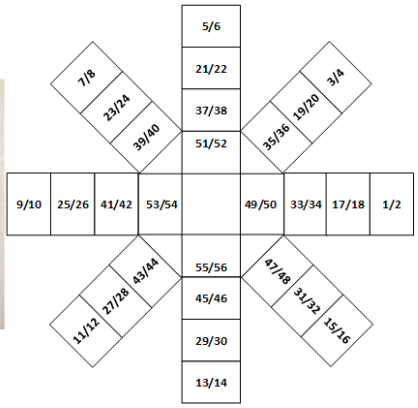

(b) Rx: 8 adjacent sides with 3 patches each, a top surface with 4 patches, each patch contains a pair of cross-polarized antennas.

Fig. 2. Antenna layouts used in the measurement

is perpendicular to them. In this measurement, the Elektrobit Propsound channel sounder was used to collect channel impulse response (CIR), and the carrier frequency is set at 3.5 GHz with 200 MHz bandwidth.

In the measurement, a 32-element uniform planar array (UPA) was used in the Tx side, and a 16-element dual-polarized omnidirectional array (ODA) was used at the MS side (see Fig. 2). In each route, the ODA was pushed with a constant speed of nearly 1.4 m/s on the 8 m rail to simulate the

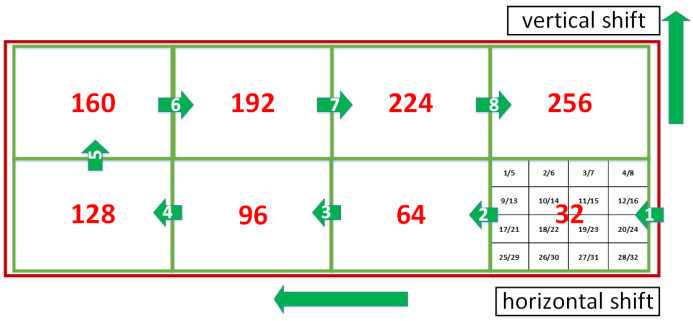

Fig. 3. The scheme of the antenna combining array in the virtual measurement

TABLE I
THE SPECIFICATIONS OF MEASUREMENT

Antenna type		ODA (MS)	UPA (Tx)
Antenna number		16	32
Overall radiation pattern		Omnidirectional	Hemispherical
Inter element spacing		41.0 mm	41.0 mm
Polarized		$\pm 45°$	$\pm 45°$
Angle range	**Azimuth**	$-180^o \sim 180^o$	$-70^o \sim 70^o$
	Elevation	$-70^o \sim 90^o$	$-70^o \sim 70^o$
Center frequency		3.5 GHz	
Bandwidth		200 MHz	
PN sequence		255 chips	

mobile condition. The specific parameters of the measurement are listed in Table I.

B. Data Processing

Firstly, we need to preprocess the data. To form the massive MIMO array with different antenna number, a virtual measurement method is adopted. Fig. 3 shows the combining scheme, giving 8 adjacent positions. For example, if we want to get the data of 64-element virtual antenna array, 2 groups of CIRs collected from 2 adjacent positions would be chosen and combined into one group of data. Then we use it as equivalent data collected from 64-element antenna array for further analysis. Similarly, to get the data of 256-element virtual antenna array, we should reorder the 8 groups of CIRs to one group, and reordering 4 groups of CIRs to get the data of 128-element virtual antenna array. By the above process, the data of 256, 128, 64 and 32-element antenna array could be gotten. The rationality of the virtual measurement is proved in [11], the power delay profile (PDP) calculated from combined CIRs and CIRs collected from the measurement campaigns can fit well. Also the spatial angular characteristics, the elevation angle of departure (EoD), azimuth of departure (AoD), elevation angle of arrival (EoA) and azimuth of arrival (AoA), which are estimated from the combination match well with those from measurement campaigns.

Secondly, to estimate the channel parameters, the SAGE algorithm is used [12], which proves to be powerful for processing of measurement data. SAGE provides a joint estimation of

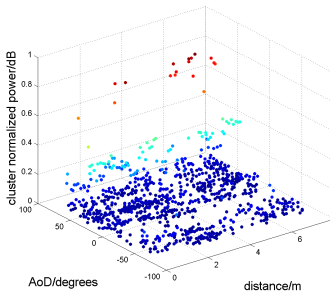

(a) 32

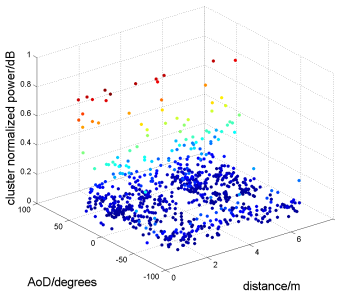

(b) 64

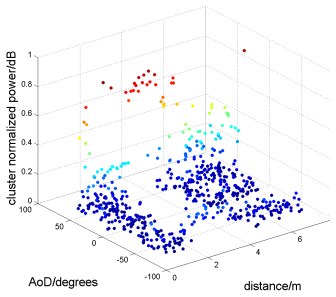

(c) 128

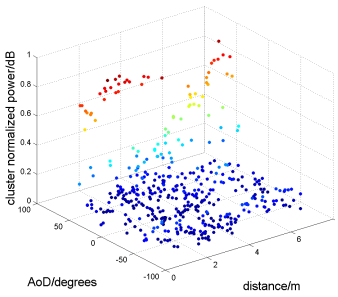

(d) 256

Fig. 4. 3D cluster-level APS of AoD in NLoS conditions

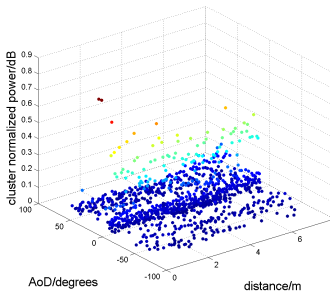

(a) 32

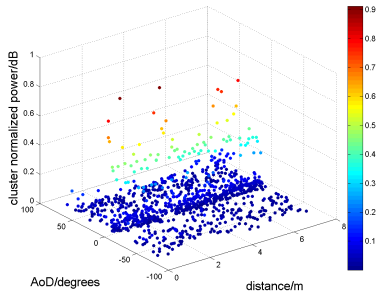

(b) 64

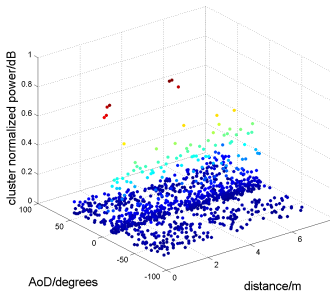

(c) 128

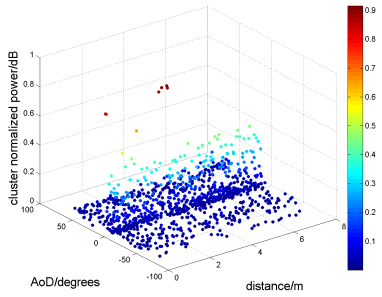

(d) 256

Fig. 5. 3D cluster-level APS of AoD in LoS conditions

parameter set $\theta_l = \{\tau_l, f_{d,l}, \Phi_l, \Omega_l, \alpha_l\}$, $l = \{1, \ldots, L\}$. The τ_l, $f_{d,l}$, Φ_l, Ω_l and α_l denote the propagation delay, the doppler shift, the angle of departure, the angle of arrival and polarization of the l-th propagation sub-path, respectively. Specifically, $\Phi_l = [\theta_{T,l}, \phi_{T,l}]$, $\Omega_l = [\theta_{R,l}, \phi_{R,l}]$, where $\theta_{T,l}$, $\phi_{T,l}$, $\theta_{R,l}$ and $\phi_{R,l}$ denote the elevation angle of departure (EoD), AoD, elevation angle of arrival (EoA) and AoA, respectively. Every 4 snapshots are fed to SAGE to estimate one parameter set.

Finally, to observe the characteristics of clusters, the KpowerMeans clustering algorithm was used to get cluster-level parameters [4, 6]. The multiple path component distance (MCD) is the distance measure for different paths in KpowerMeans. It is a normalized value composing of delay and angular parts. For delay distance, the definition is given as

$$MCD_{\tau,ij} = \eta \cdot \frac{|\tau_i - \tau_j|}{\Delta\tau} \cdot \frac{\tau_{sd}}{\Delta\tau} \tag{1}$$

In this equation, η is a scaling factor to adjust the weight of delay in the distance function. $\Delta\tau$ means the range of delay and $\Delta\tau = max_{i,j}|\tau_i - \tau_j|$. τ_{sd} is the standard deviation of delay.

For angle distance, the definition is given as

$$MCD_{T/R,ij} = \frac{1}{2}\left| \begin{pmatrix} sin(\theta_i)cos(\varphi_i) \\ sin(\theta_i)sin(\varphi_i) \\ cos(\theta_i) \end{pmatrix} - \begin{pmatrix} sin(\theta_j)cos(\varphi_j) \\ sin(\theta_j)sin(\varphi_j) \\ cos(\theta_j) \end{pmatrix} \right| \tag{2}$$

For TX or RX, the angle distance is obtained in the spherical coordinate system. θ means the elevation angle and φ means the azimuth angle.

The total distance is given by

$$MCD_{ij} = \sqrt{\left\|MCD_{T,ij}\right\|^2 + \left\|MCD_{R,ij}\right\|^2 + \left\|MCD_{\tau,ij}\right\|^2} \tag{3}$$

We can see from above equations that MCD consists of three parts, angle of arrival, angle of departure, delay.

1) Delay Spread: the delay spread can be calculated by

$$\tau_{rms,k} = \sqrt{\sum_{l=1}^{L_k} \tau_{l,k}^2 \cdot P_{l,k} / \sum_{l=1}^{L_k} P_{l,k} - \mu_{\tau,k}^2} \tag{4}$$

where $\tau_{l,k}$ is the excess delay of the lth path of the kth cluster. L_k is the total path number fot the kth cluster. $P_{l,k}$ is the cluster power of the lth path of the kth cluster. $\mu_{\tau,k}$ is the mean value of the kth cluster's delay, which is given by

$$\mu_{\tau,k} = \sum_{l=1}^{L_k} \tau_{l,k} \cdot P_{l,k} / \sum_{l=1}^{L_k} P_{l,k} \tag{5}$$

2) Angular Spread:

$$\sigma_{AS,k} = \sqrt{\sum_{l=1}^{L_k} (\varphi_{l,k} - \mu_k)^2 \cdot P_{l,k} / \sum_{l=1}^{L_k} P_{l,k}} \tag{6}$$

where $\varphi_{l,k}$ denotes the angle degree of the lth path of the kth cluster. μ_k is the mean value of the kth cluster, which is given by

$$\mu_k = (\sum_{l=1}^{L_k})\varphi_{l,k} \cdot P_{l,k} / (\sum_{l=1}^{L_k} P_{l,k}) \tag{7}$$

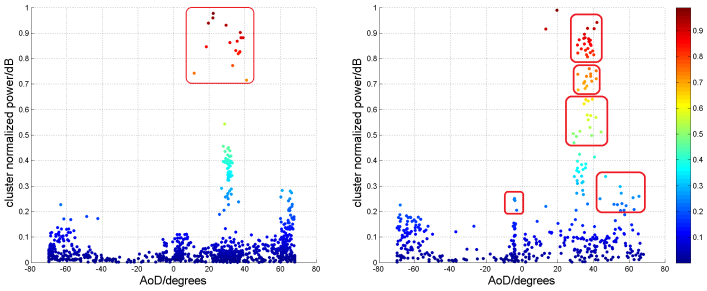

(a) 32 (b) 256

Fig. 6. cluster-level APS on Y-Z axis in NLoS conditions

TABLE II
THE INTRA-CLUSTER PARAMETERS OF MEASUREMENT

Antenna Number		ASD		ASA		DS	
		μ	σ	μ	σ	μ	σ
LoS	32	7.0	5.5	13.4	11.2	6.1	2.4
	64	6.9	6.1	10.5	11.9	7.2	4.1
	128	6.5	6.3	9.1	11.0	6.5	4.2
	256	6.6	6.5	6.8	8.4	6.9	3.6
NLoS	32	6.1	5.8	12.2	11.6	13.9	44.6
	64	7.4	6.2	9.4	12.0	15.5	39.5
	128	8.7	6.6	9.4	12.3	23.1	50.1
	256	9.7	7.2	7.4	9.2	31.0	65.5

III. ANALYSIS OF THE MEASUREMENT DATA

A. The distribution of clusters

By observing the 3D angular power spectrum (APS), the spatial variation of clusters along with the measurement route, and cluster variation with the increasing number of antennas can be shown. Fig. 4 and Fig. 5 shows 4 cluster-level 3D APSs of AoD with 32, 64, 128 and 256-element antenna array in NLoS and LoS conditions, respectively. In these figures, every point represents the spatial position of one cluster, X-coordinate represents distance from the starting point of the rail, Y-coordinate represents the angular degree of the cluster, Z-coordinate and the color of the points represents the normalized power of clusters. So clusters with different power show in different colors, we name them 'color cluster', e.g., clusters which power is $>$0.8 called 'red clusters'.

As shown in Fig. 4, 4 groups of clusters distribute in different degrees along with the measurement route. Most of clusters are 'deep blue clusters', their power is low. During the movement, the clusters' positions and power keep changing . We can see that when antennas become more, the power of clusters has an increasing trend. In Fig. 4 (a), only a few of red clusters, while in Fig. 4 (b), red clusters become more. When antenna number become 128 and 256, the orange, yellow and green clusters appear in some distances and their number become more. In the meantime, the distribution of the deep blue clusters becomes sparser when antennas increase. This is because when Tx has more antennas, Tx would have better condition of transmitting, so the lifetimes of clusters become longer during movement and the power of clusters become higher. A similar phenomenon is shown in LoS conditions (see Fig. 5). Most of clusters focus on the LoS path in $0°$. In the measurement, R1 is parallel to the transmitting waves. So the increasing trend of cluster power is not as obvious as that in NLoS conditions when antenna number increases. In Fig. 6, the APSs are shown on Y-Z axis in NLoS conditons, which present the relation between power and angles. In Fig. 6 (b), on the degrees ranging from $40°$ to $60°$ and near $0°$, it appears more new light blue clusters than that in Fig. 6 (a).

The APS also shows that the concentration positions of angles will change with different antenna number. Compared Fig. 6 (a) with Fig. 6 (b), we can see that with more antennas, more and more clusters distribute on degrees ranging from $20°$ to $40°$. When the antennas become 256, red , orange and yellow clusters become more and get focus on the degrees ranging from $30°$ to $40°$, while there is no yellow clusters and less red and orange clusters in 32 antennas case.

So it can be concluded that when the number of antenna increases, the clusters will become more, and the total power of clusters will become higher. In NLoS conditions, the concentration positions of angles will shift slightly.

B. the intra-cluster AS and DS

By using the equations (4) - (7), the intra-cluster parameters including cluster-level ASD, ASA and DS are calculated. Considering the mobile measurement, the clusters changes along with the route. These parameters are calculated every 4 snapshots, then their mean value μ and standard deviation σ are given in Table II. In NLoS conditions, ASD tends to become more and ASA tends to become less when the antenna number increases while ASD and ASA changes slightly in LoS conditions. R1 is parallel to the transmitting waves, so when the antennas increase, the added antennas have marginal effect on the channel. R2 is perpendicular to the transmitting waves, and its LoS path is blocked by the building. The added antennas will provide more paths to the channel. So at Tx side, ASD become bigger, and ASA become smaller at MS side. And DS becomes larger as the antennas increase. These trends denote that larger antenna array at Tx side will provide more scattering paths in mobile channel.

Fig. 7 (a) and (b) plot the CDFs of ASD and ASA in NLoS conditions, respectively. The result shows that the ASD increases with the number of antennas, the 256-element virtual array has the biggest ASD. And the median values (50%) of ASD accords with the trend (see Table II). ASA shows the opposite result, it becomes smaller as the antennas increase. These trends in these two figures is same as those in Fig. 4, 5 and 6.

The intra-cluster parameters including ASD, ASA and DS are listed in Table III. In LoS conditions, the variation of DS among different number of antennas is slight, while increasing trend of DS is obvious in NLoS conditions. What is more, comparing NLoS conditions with LoS conditions, mainly of ASD and DS are larger, and ASA is smaller.

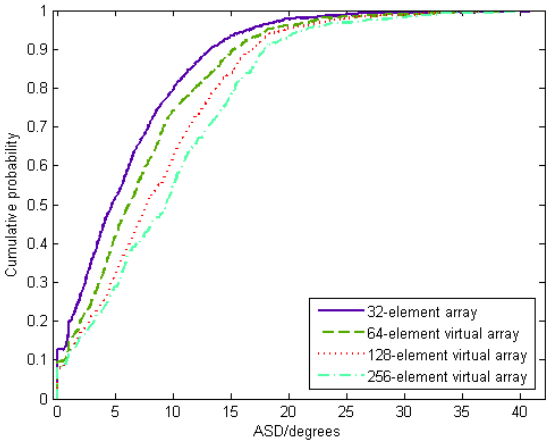

(a) ASD

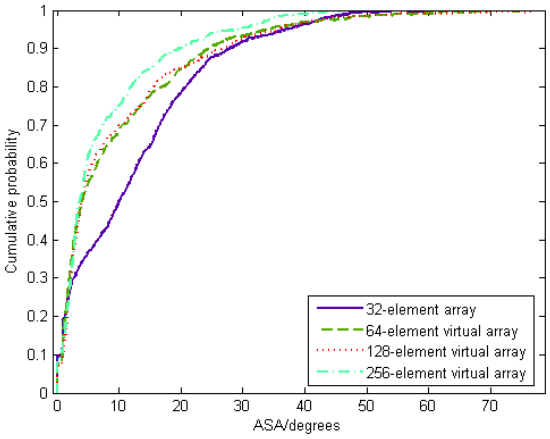

(b) ASA

Fig. 7. the CDFs of ASA and ASD in NLOS conditions

TABLE III
THE MEDIAN VALUE OF THE CDF OF AS

	32	64	128	256
ASD (°)	4.70	6.18	7.66	9.38
ASA (°)	10.00	4.00	3.91	3.58

IV. CONCLUSION

In this paper, a massive MIMO mobile measurement at 3.5 GHz, in LoS and NLoS conditions, respectively, was performed for cluster analysis. By virtual measurement method, the 32-element antenna array can be used to form the 64-element, 128-element and 256-element virtual antenna array. Then the data is analyzed, comparing these 4 groups of data in angle domain and delay domain.

It can be concluded that with the increasing number of antennas, the clusters' power will become higher, especially in some strong path. In NLoS conditions, clusters appear in new paths, some paths become stronger. In the meantime, intra-cluster ASD becomes larger and intra-cluster ASA becomes smaller, which denotes the better channel capacity in massive MIMO. DS becomes larger, which denotes that the paths become more.

ACKNOWLEDGMENT

This research is supported in part by National Science and Technology Major Project of the Ministry of Science and Technology (2014ZX03003013), and in part by National Key Technology Research and Development Program (2012BAF14B01), and in part by National Natural Science Foundation of China (61322110, 6141101115), and by 863 Program (2015AA01A703) and Doctoral Fund of Ministry of Education (201300051100013). This research is also supported by Huawei Technologies Co., Ltd.

REFERENCES

[1] A. Molisch, "Modeling the MIMO propagation channel," *Beigian Journal of Electronics and Communications*, no. 4, pp. 5-14, 2003.
[2] L. Correia, Ed., "Mobile Broadband Multimedia Netwoks." Published by *Acadamic Press*, 2006.
[3] K. Li, M. Ingram, and A. Van Nguyen, "Impact of clustering in statistical indoor propagation models on link capacity," *IEEE Trans. Commun.*, vol. 50, no. 4, pp. 521-523. April 2002.
[4] D. Du, J. Zhang, C. Pan and C. Zhang, "Cluster Characteristics of Wideband 3D MIMO Channels in Outdoor-to-Indoor Scenario at 3.5 GHz," *2014 IEEE 79th Vehicular Technology Conference (VTC Spring)*, Seoul, 2014, pp. 1-6.
[5] X. Yin, C. Ling and M. D. Kim, "Experimental Multipath-Cluster Characteristics of 28-GHz Propagation Channel," *IEEE Access*, vol. 3, no. , pp. 3138-3150, 2015.
[6] C. Huang, J. Zhang, X. Nie and Y. Zhang, "Cluster Characteristics of Wideband MIMO Channel in Indoor Hotspot Scenario at 2.35GHz," *Vehicular Technology Conference Fall (VTC 2009-Fall), 2009 IEEE 70th*, Anchorage, AK, 2009, pp. 1-5.
[7] X. Gao, O. Edfors, F. Rusek, and F. Tufvesson, "Massive MIMO performance evaluation based on measured propagation data," *IEEE Trans. Wireless Commun.*, vol. 14, no. 7, pp. 3899-3911, Jul. 2015
[8] E. G. Larsson, O. Edfors, F. Tufvesson, and T. L. Marzetta, "Massive MIMO for next generation wireless systems," *IEEE Commun. Mag.*, vol. 52, no. 2, pp. 186-195, Feb. 2014.
[9] X. Gao, F. Tufvesson and O. Edfors, "Massive MIMO channels - Measurements and models," *2013 Asilomar Conf. on Sig., Systems and Comp.*, Pacific Grove, CA, 2013, pp. 280-284.
[10] W. Li, L. Liu, C. Tao, Y. Lu, J. Xiao and P. Liu, "Channel measurements and angle estimation for massive MIMO systems in a stadium," *2015 17th International Conf. on Advanced Commu. Tech. (ICACT)*, Seoul, 2015, pp. 105-108.
[11] H. Yu, J. Zhang, Q. Zheng, Z. Zheng, L. Tian and Y. Wu, "The rationality analysis of masssive MIMO virtual measurement at 3.5 GHz", *2016 Workshop, IEEE International Conf. on Comp. and Commu.* (ICCC Workshop), in press.
[12] B. Fleury, M. Tschudin, R. Heddergott, D. Dahlhaus, and K. Ingeman Pedersen, "Channel parameter estimation in mobile radio environments using the SAGE algorithm," *IEEE J. Sel. Areas in Commun.*, vol. 17, no. 3, pp. 434-450, Mar. 1999.